ORIGINAL RESEARCH

In vivo osseointegration of Ti implants with a strontium-containing nanotubular coating

Yonggang Dang[1]
Li Zhang[1]
Wen Song[1]
Bei Chang[1]
Tianxiao Han[1]
Yumei Zhang[1]
Lingzhou Zhao[2]

[1]Department of Prosthetic Dentistry,
[2]Department of Periodontology,
School of Stomatology, State Key
Laboratory of Military Stomatology,
The Fourth Military Medical
University, Xi'an, People's Republic
of China

Abstract: Novel biomedical titanium (Ti) implants with high osteogenic ability for fast and good osseointegration under normal as well as osteoporotic conditions are urgently needed. Expanding on our previous in vitro results, we hypothesized that nanotubular, strontium-loaded (NT-Sr) structures on Ti implants would have favorable osteogenic effects and evaluated the in vivo osseointegration of these implants in rats. The structures with nanotubes of different diameters were fabricated by electrochemical anodization at 10 and 40 V, and the amounts of Sr loaded were adjusted by using two hydrothermal treatment times of 1 and 3 hours. Qualitative microcomputed tomography in two and three dimensions showed that the NT-Sr formed with an anodization voltage of 10 V and hydrothermal treatment time of 3 hours best supported bone growth in vivo. Histomorphometric examination of osseointegration also showed that more newly formed bone was found at its surface. The bone–implant contact percentage was highest (92.48%±0.76%) at 12 weeks. In conclusion, the NT-Sr formed with an anodization voltage of 10 V and hydrothermal treatment time of 3 hours showed excellent osteogenic properties, making it an attractive option for Ti surface modification with considerable clinical potential.
Keywords: titania nanotubes, strontium, osseointegration, in vivo

Introduction

Titanium (Ti) implants are important therapeutic tools broadly utilized in orthopedic and dental applications. Although relatively high success rates are achieved in procedures employing these materials, many issues persist, primarily related to unsatisfactory osseointegration of Ti implants. For example, a long healing period of 3–6 months is needed before final prosthetic restoration and functional loading are possible in treatments involving Ti dental implants, which causes much inconvenience to patients. Even more problematic is implant failure due to insufficient osseointegration. It is reported that more than 20% of total hip replacements must be repeated within 10–14 years after the initial surgery.[1] Moreover, the incidence of osteoporosis arising from various causes continues to increase, and the corresponding low bone quality, high bone turnover, and negative bone remodeling balance compromises implant osseointegration in these patients.[2,3] Therefore, advanced implants with the capability of modulating bone turnover toward osteogenesis to rapidly achieve rigid and long-lasting osseointegration are needed to further improve the clinical success rate of implant surgeries, prolong the life span of implants, and extend their applicability in patients with osteoporosis.

Nanotopographical modifications specifically designed to emulate the properties of natural extracellular matrix and for bioactive element delivery represent an effective method for improving the bioactivity of biomaterials.[4] For example, titania

Correspondence: Lingzhou Zhao
Department of Periodontology, School
of Stomatology, State Key Laboratory
of Military Stomatology, The Fourth
Military Medical University, No 145 West
Changle Road, Xi'an 710032, People's
Republic of China
Email zhaolingzhou1983@hotmail.com

Yumei Zhang
Department of Prosthetic Dentistry,
School of Stomatology, State Key
Laboratory of Military Stomatology,
The Fourth Military Medical University,
No 145 West Changle Road, Xi'an
710032, People's Republic of China
Email wqtzym@fmmu.edu.cn

nanotubes (NTs), which can be fabricated with precisely controlled diameters and lengths to mimic natural bone tissues and with an elasticity similar to that of bone,[5,6] can selectively induce differentiation of mesenchymal stem cells (MSCs) down the bone lineage.[4,7,8] In vivo studies have also confirmed that surfaces modified with NTs can achieve enhanced osseointegration.[9–11] In addition, NTs constitute an excellent drug delivery platform through which bioactive elements may be delivered to further augment osteogenesis and osseointegration at the implant interface.[12–17]

Strontium (Sr) has been shown to increase osteoblast replication and differentiation and bone matrix mineralization, probably via a calcium-sensing receptor-dependent mechanism,[18–21] and has also been reported to induce MSC commitment to the bone lineage.[22–26] At the same time, Sr can inhibit bone resorption by reducing the osteoblast production of matrix metalloproteinase, reducing osteoclast differentiation and resorption activity, and inducing osteoclast apoptosis.[18,20,27] Thus, constant in situ release of Sr at a proper dose directly at the implant–tissue interface has been proposed to enhance the implant osseointegration, and multiple recent studies have investigated the benefits of Sr loading onto biomaterials.[21,28–31] On the basis of the hypothesis that the combination of an appropriate NT-coated surface and controllable, long-term Sr release may give rise to a material with an enhanced ability to promote osteogenesis and thus achieve rigid implant osseointegration, we developed a series of NT-coated, Sr-loaded Ti samples and found that the NT-Sr structure with suitable Sr loading led to improved proliferation, spreading, and osteogenic differentiation of in vitro cultured MSCs.[32] Although our in vitro results were promising, in vivo observations are necessary to draw a final conclusion on the osseointegration ability of a biomaterial. Therefore, we systemically evaluated the in vivo osseointegration ability of Ti implants modified with the NT-Sr structure.

Materials and methods
Implant fabrication

Custom screw implants made of commercially pure titanium (cpTi), measuring 3 mm in diameter and 6 mm in length, were used for the histological analyses of implant osseointegration. Custom cylindrical implants of cpTi, measuring 1 mm in diameter and 12 mm in length, were used for the pull-out test. The Ti implants were grit-blasted and ultrasonically cleaned with acetone, ethanol, and deionized water sequentially. They were then treated by electrochemical anodization in

an ethylene glycol solution with 0.5 wt% NH_4F, 5 vol% CH_3OH, and 5 vol% H_2O at 10 V for 1 hour or 40 V for 40 minutes, with the formed samples designated as NT10 and NT40, respectively. To fabricate the NT-Sr samples, NT10 and NT40 samples were further placed in 40 mL of 0.02 M $Sr(OH)_2$ solution in a 60 mL Teflon-lined autoclave and heated at 200°C for 1 or 3 hours under controlled pressure, with the formed samples designated as NT10-Sr1, NT10-Sr3, NT40-Sr1, and NT40-Sr3, respectively. The fabricated Ti samples were ultrasonically washed with 1 M HCl for 5 minutes to remove the residual $Sr(OH)_2$, rinsed with distilled water, and finally dried in air. Grit-blasted Ti samples served as the control Ti surface. The samples were characterized by field-emission scanning electron microscopy (FE-SEM, HITACHI S-4800, Hitachi, Tokyo, Japan). The Ti implants were stored at room temperature and sterilized by ^{60}Co irradiation before implantation.

Animals and surgical procedure

The animal experiments were performed in accordance with the international standards on experimental animal welfare, and the protocols were reviewed and approved by the Animal Research Committee of The Fourth Military Medical University, People's Republic of China. Twenty-eight female Sprague Dawley rats, aged 3 months and weighing approximately 240 g were provided by the Laboratory Animal Research Centre of the Fourth Military Medical University. The animals were housed two per cage in a climate-controlled environment at 25°C, 55% humidity, and 12-hour alternating light–dark cycle. Free access to standard laboratory diet and tap water was provided. All animals were acclimatized for 2 weeks before use in this study. The 28 rats were randomly assigned to 7 groups (n=4 each) to receive different types of implants. The screw and cylindrical implants were placed into the bilateral femoral and tibial condyles, respectively.

All of the surgeries were performed under general anesthesia achieved via intraperitoneal injection of pentobarbital (30 mg/kg) under sterile conditions. The animals were immobilized supinely, and the hind limbs were shaved, washed, and disinfected with 10% povidone iodine. A midline longitudinal parapatellar incision was made, and the knee joint capsule was incised longitudinally. After the patellar ligament was lifted gently and moved laterally, the knee joint was exposed, and this was facilitated by a slight extension of the knee. For placement of the screw implant, at the intercondylar notch of the femur, a cylindrical hole of 3 mm in diameter was prepared parallel to the long axis of

the bone using dental burs and a surgical motor (OsseoSet 200, Nobel Biocare AB, Gothenburg, Sweden) with a low rotational drill speed (800 rpm) and continuous external cooling with saline. Similarly, a cylindrical hole of 1 mm in diameter was prepared at the intercondylar notch of tibia for the implantation of a cylindrical sample. After insertion of the implants, the soft tissue layers and skin were closed with sutures. After the operation, gentamicin (1 mg/kg) was administrated intramuscularly for 5 continuous days, and animals were monitored on a daily basis. After completion of the implantation procedures, all the rats had free access to normal pellet food and water.

Twelve weeks after implant insertion, the femurs and tibias containing the implants were harvested for evaluation according to the biomechanical pull-out test, microcomputed tomography (CT), histological, and histomorphometric staining. After careful dissection and cleaning of any adhering soft tissues, the tibia samples were immediately subjected to biomechanical push-out tests. The femurs were fixed in neutral buffered formaldehyde for 48 hours and then preserved in 70% ethanol for micro-CT evaluation as well as the histological analysis of undecalcified specimens.

X-ray evaluation of bone healing

At 4 and 12 weeks after implant insertion and immediately before the rats were sacrificed, the bone around the implants was examined by X-ray imaging.

Biomechanical pull-out test

The biomechanical pull-out test was conducted immediately after the tibias with the cylindrical implants were harvested. The tests were performed using a universal material testing system (AGS-10 kN, Shimadzu, Kyoto, Japan). A special customized holder was applied to fix the test samples to ensure that the test force was exerted along the long axis of the implants, and the tibias were trimmed to fit the holder. All tests were performed at a strain rate of 1 mm/min. The load–displacement curve was recorded, and the failure load was defined as the peak load value of the load–displacement curve.

Micro-CT evaluation

For quantitative three-dimensional (3D) analysis on implant osseointegration, bone samples (n=4 per group) were scanned using a micro-CT system (Inveon, Siemens, Erlangen, Germany; 80 kV, 100 mA, 800 ms integration time) and reconstructed with an isotropic voxel size of 30 μm.

The 3D images reconstructed from the microtomographic slices were used for quantitative evaluation. Each region of interest (ROI) was chosen along the implant length using the Siemens Research Workplace software (Siemens). Each ROI was a cylinder in the area of the metaphysis with a diameter of 3.2 mm and a height of 2 mm and included the entire implant structure and 0.1 mm of the surrounding bone tissue. For all images, a threshold was manually selected to isolate bone tissue and preserve its morphology. Trabecular thickness (Tb.Th), trabecular number (Tb.N), trabecular spacing (Tb.Sp), trabecular pattern factor (Tb.P.F), bone surface area/ bone volume (BS/BV), and bone volume/total volume ratio (BV/TV) were determined.

Histological analysis and histomorphometry

To evaluate the bone response around the implants, histological and histomorphometric analyses were conducted. The sections were prepared as described in the "Micro-CT evaluation" section and then stained by Van–Greson staining. Histological evaluation was carried out using a light microscope (DM6000B, Leica Microsystems, Wetzlar, Germany). For the histomorphometric analysis, a computer-based image analysis system (Leica LAS AF, Leica Microsystems) was used. The bone-to-implant contact ratio (BIC, %) was calculated at 10× magnification for three different sections per implant. Each ROI was defined in the area of the metaphysis along one side of the implant to exclude the growth plate area and inferior cortical bone of the femoral condyle.

Statistical analysis

All statistical analyses were carried out using SPSS 12.0 (SPSS Inc., Chicago, IL, USA). The data are presented as mean ± standard deviation values. One-way analysis of variance and Student–Newman–Keuls post hoc tests were used to determine the level of significance, and P-values <0.05 and <0.01 were considered to be significant and highly significant, respectively.

Results
Structure characterization

The SEM images in Figure 1 show an even distribution of vertically aligned NTs on the treated Ti samples. The NT diameters on the NT10 and NT40 samples were 30 and 80 nm, respectively, indicating that the size of the NTs was dependent on the anodization voltage. After hydrothermal treatment in the $Sr(OH)_2$ solution, the nanotubular
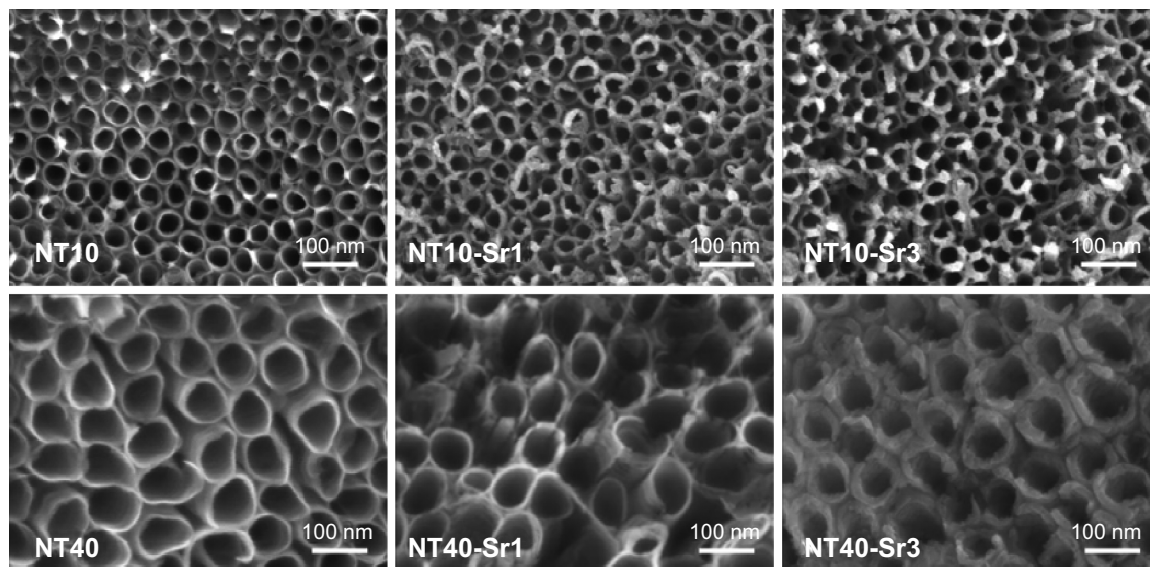
Figure 1 Representative FE-SEM images of Ti surfaces modified with NT and NT-Sr structures.
Abbreviations: FE-SEM, field-emission scanning electron microscopy; NT, nanotube; Sr, strontium; Ti, titanium.

architecture was well preserved, but notably, the NT diameter decreased while the NT walls became thicker with increasing treatment time.

Clinical observations following implantation

After the implantation surgeries, all rats were able to walk normally within 12 hours after surgery. No signs of inflammation or adverse reactions were observed, and none of the rats died or suffered a bone fracture during the study.

X-ray evaluation of bone healing

At 4 and 12 weeks after implant insertion and immediately before the rats were sacrificed, the healing condition of the implants was examined by X-ray imaging. The representative X-ray images (shown in Figure 2) displayed normal healing around all implants, with no discernible signs of bone resorption.

Biomechanical pull-out strength

Biomechanical pull-out testing was used to evaluate the quality of the established implant osseointegration (Figure 3). At 12 weeks, compared to that for Ti control samples, the failure loads for NT and NT-Sr samples were higher. In general, all NT-Sr samples, except NT10-Sr1, showed a higher failure load than the Sr-free counterparts. Notably, the failure load for the NT10-Sr3 samples was higher than those for the NT10 and NT40-Sr1 samples. Moreover, the failure load was higher for the NT40-Sr3 samples than for

the NT40 samples. Overall, the 40 N failure load for the NT10-Sr3 sample was the highest at 12 weeks.

Micro-CT evaluation of osseointegration

The qualitative micro-CT two-dimensional and 3D images shown in Figures 4 and 5 provide information regarding implant osseointegration and the peri-implant trabecular microstructure. The corresponding qualitative BV measurements for all experimental groups are presented in Figure 6. Compared with the other experimental implants, the NT10-Sr3 implants showed the best effects with regard to increasing BV in the metaphysis.

Histological and histomorphometric examination of osseointegration

At 12 weeks, little bone formation was observed surrounding the implants in the control group. More newly formed bone was found at the surface of the NT10-Sr3 implants, indicating better osseointegration (Figure 7). The BIC percentage for the NT10-Sr3 implant was highest among the experimental groups (92.48%±0.76%) at 12 weeks (Figure 8).

Discussion

The physicochemical characteristics of a coating material play an important role in the overall bioactivity of coated Ti implants as well as in mediating cellular function on the implant surface. Both surface chemistry and topography significantly influence the speed and extent of osseointegration of biomedical implants. A surface modification strategy
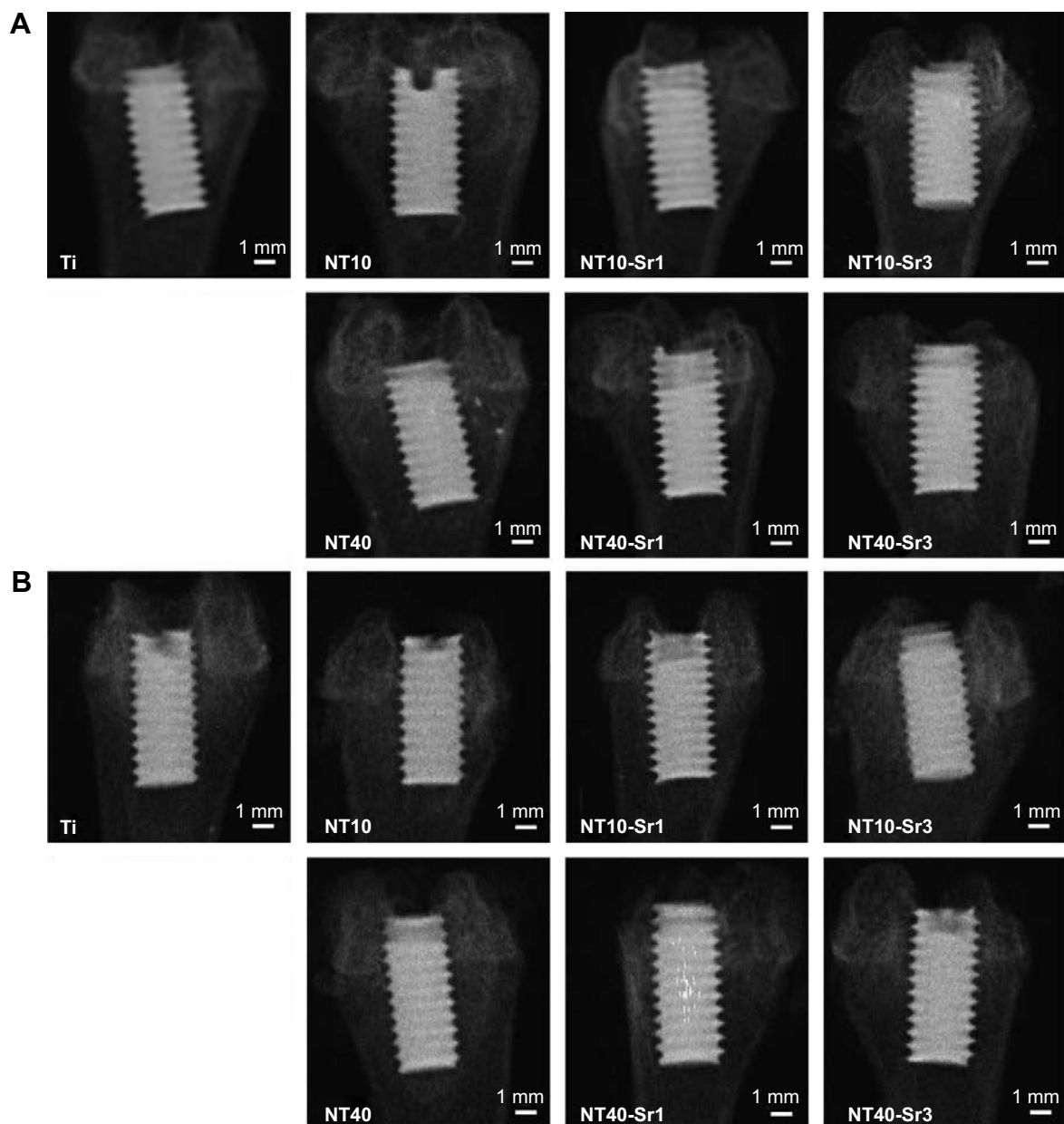
Figure 2 Representative X-ray images of NT, NT-Sr, and Ti control samples 4 weeks (**A**) and 12 weeks (**B**) after bony implantation.
Abbreviations: NT, nanotube; Sr, strontium; Ti, titanium.

that combines the use of bioactive trace elements together with surface micro-/nanotopographical modification was employed in this study, with the goal of enhancing the osseointegration of Ti implants. Ti implants that contain Sr are considered promising for clinical use, because the Sr stimulates bone formation and prevents bone absorption, leading to the accelerated osseointegration.

The three essential steps for bone formation are cellular osteogenic differentiation, matrix maturation, and matrix mineralization. The initial adhesion of cells to an implant is a key step for cell proliferation and differentiation on a biomaterial.

Our previous study demonstrated in vitro that the protein deposition pattern can be influenced by the implant surface nanotopography,[4] which in turn can affect the biological performance of biomaterials. Our early research showed that with regard to NT10, the abundant and relatively evenly distributed nanoscale protein bundles allow for the formation of high-quality focal adhesions. However, NT40 that has relatively sparsely distributed nanoscale protein pillars does not support cell adhesion well, because the focal adhesion will mostly, and maybe even totally, be constrained to the small top ends of the protein pillars, resulting in compromised cell adhesion and spreading.
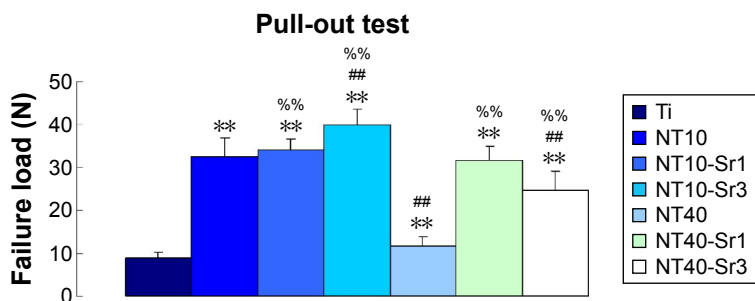
Pull-out test

Figure 3 Pull-out strength for the explanted samples.
Notes: $^{**}P<0.01$ vs Ti, $^{\#\#}P<0.01$ vs NT10, and $^{\%\%}P<0.01$ vs NT40 (n=28).
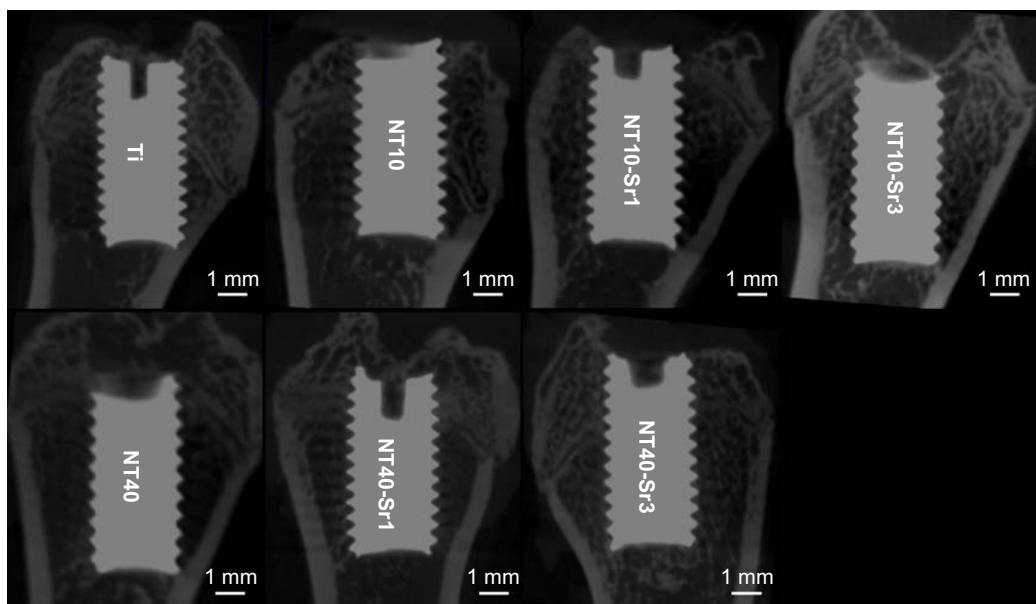**Abbreviations:** NT, nanotube; Sr, strontium; Ti, titanium.

Figure 4 Micro-CT 2D reconstructed models showing the status of the Ti implant and bone response at 12 weeks after implantation.
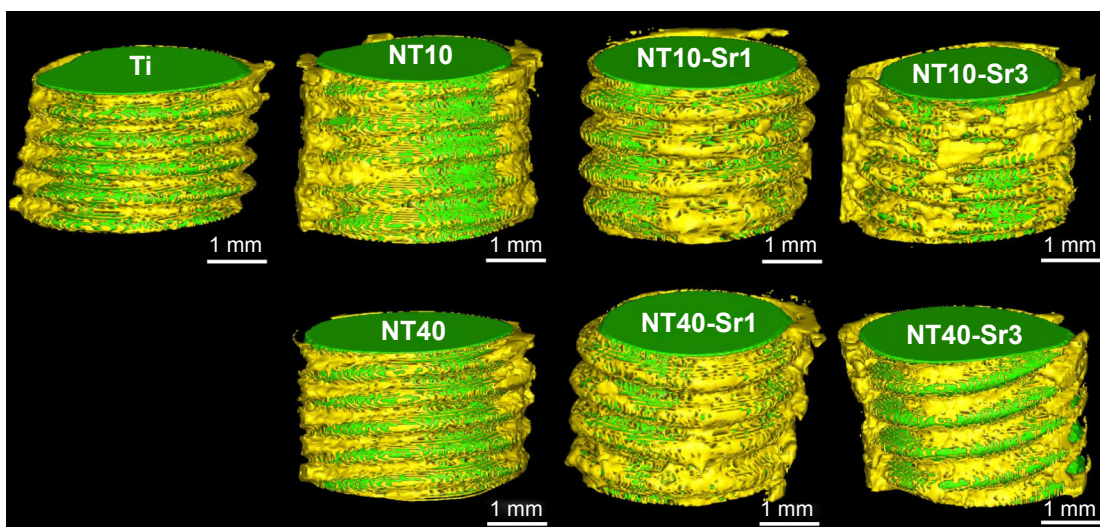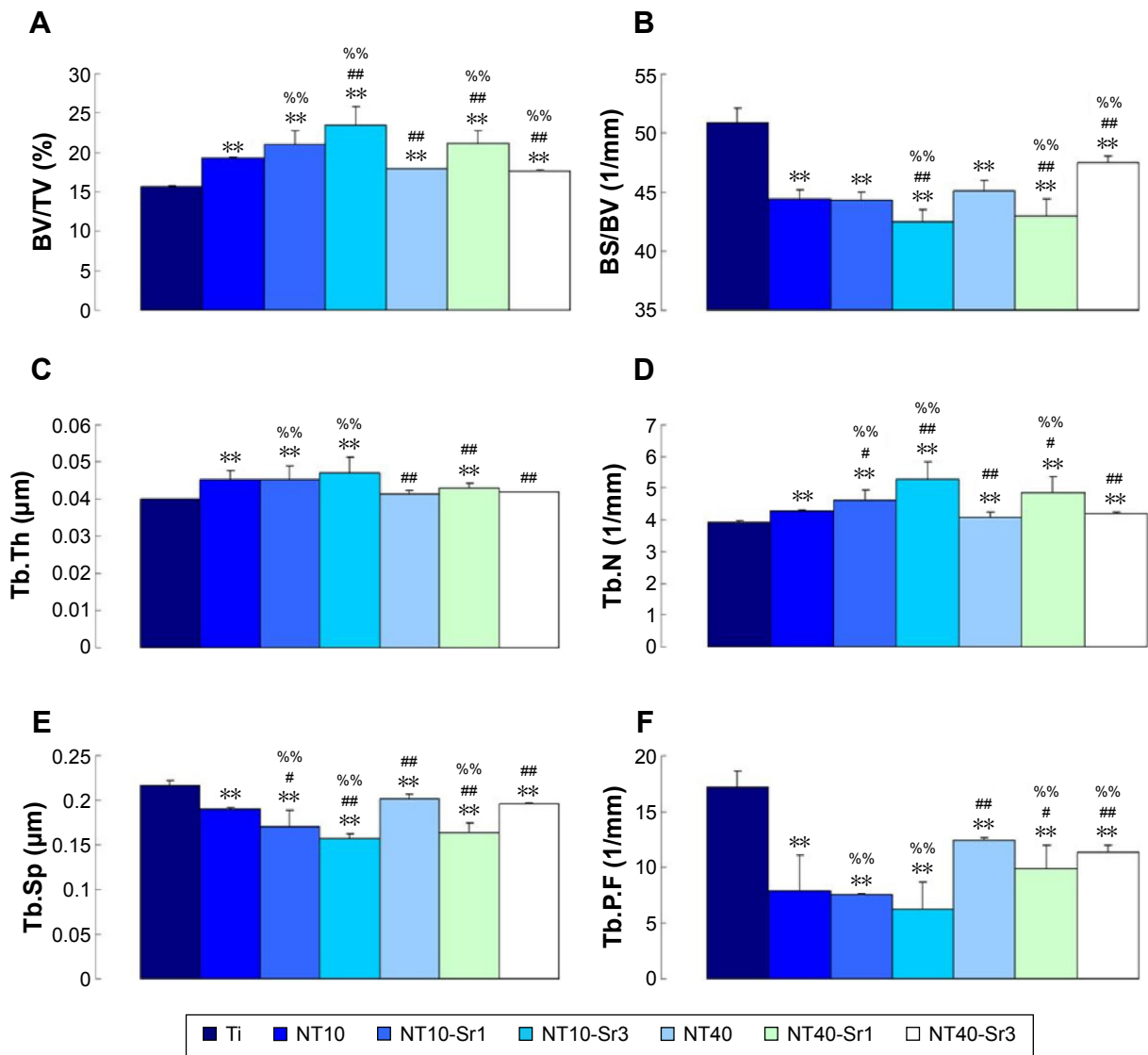**Abbreviations:** CT, computed tomography; NT, nanotube; Sr, strontium; Ti, titanium; 2D, two-dimensional.

Figure 5 Micro-CT 3D reconstructed models showing the status of the Ti implant (green in color) and the response of bone (yellow in color) at 12 weeks after implantation.
Abbreviations: CT, computed tomography; NT, nanotube; Sr, strontium; Ti, titanium; 3D, three-dimensional.

Figure 6 Micro-CT analysis of (**A**) BV/TV, (**B**) BS/BV, (**C**) Tb.Th, (**D**) Tb.N, (**E**) Tb.Sp, and (**F**) Tb.P.F.
Notes: **$P<0.01$ vs Ti, #$P<0.05$ or ##$P<0.01$ vs NT10, and %%$P<0.01$ vs NT40 (n=28).
Abbreviations: BV, bone volume; BS, bone surface area; CT, computed tomography; NT, nanotube; Sr, strontium; Tb.P.F, trabecular pattern factor; Tb.Sp, trabecular spacing; Tb.N, trabecular number; Tb.Th, trabecular thickness; Ti, titanium; TV, total volume.
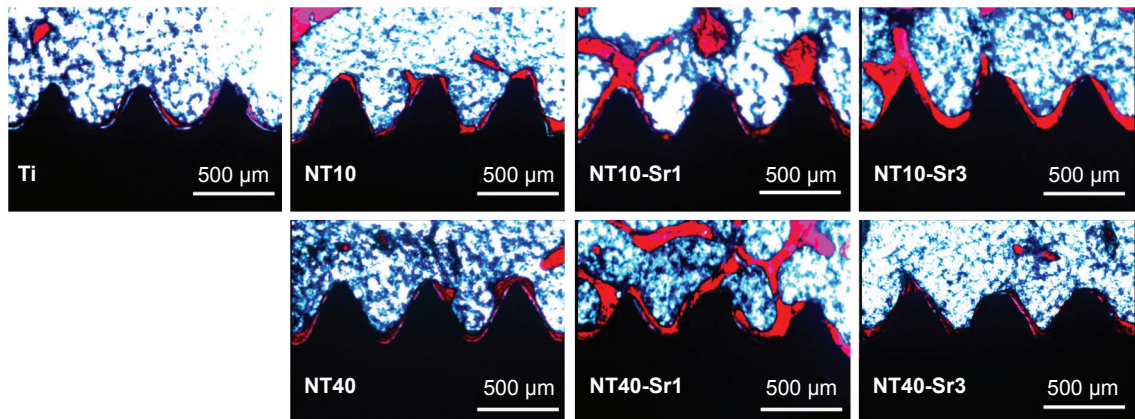

Figure 7 Representative images of VG staining showing the bone (red) formed around the Ti implant (black) at 12 weeks after implantation.
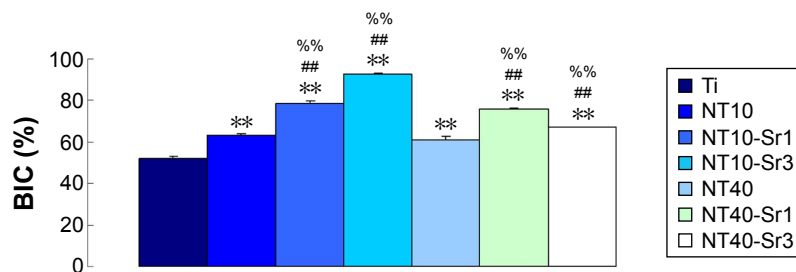**Abbreviations:** NT, nanotube; Sr, strontium; Ti, titanium; VG, Van–Greson.

Figure 8 Histomorphometrical analysis of BIC (%).
Notes: **$P<0.01$ vs Ti, ##$P<0.01$ vs NT10, and %%$P<0.01$ vs NT40 (n=28).
Abbreviations: BIC, bone–implant contact; NT, nanotube; Sr, strontium; Ti, titanium.

Most previous studies have demonstrated the dose dependency of the effects of Sr on cell proliferation, which is consistent with our results.[32] Our previous in vitro research indicated that the released Sr more strongly affects MSC osteogenic differentiation than the topography of the implant surface or cell area. Choudhary et al[24] also reported that Sr within Ti implants can induce MSC osteogenic differentiation. Thus, it is reasonable to conclude that the enhanced cell proliferation on the NT10-Sr samples in contrast to that on the NT10 samples can be attributed primarily to Sr. Moreover, the structure of the NTs allows high-quality focal adhesion formation to support cell spreading and induces the formation of large nodular alkaline phosphatase (ALP) deposits and mineralized nodules. The production of nodular ALP products and mineralized nodules can be further enhanced by Sr release, especially for NT10. Interestingly, in our experiments, Sr at an appropriate concentration loaded into Ti implants with a suitable NT array could not only increase osteogenic differentiation but also promote the secretion of extracellular matrix.

When inserted in cortical and corticocancellous bone in an in vivo murine femur implantation model, the NT10-Sr3 material demonstrated superior osseointegration compared to that observed for the NT10, NT10-Sr1, NT40, NT40-Sr, and uncoated Ti samples, with firm abutments between the implant and the surrounding skeletal tissue. Histological analysis confirmed that more new bone was formed, and the gap was filled more densely between the implants with the NT10-Sr3 material compared to the others. The BIC on NT-Sr coated implants was significantly higher, compared to that of NT and uncoated Ti, reflecting the ability of these coatings to induce osseointegration without any infiltration of fibrous tissue between the bone and implant.

Biomechanical tests (eg, pull-out/push-out, torque, or tensile test) are used to characterize the bonding strength at the bone–implant interface. The results of our pull-out testing revealed that the mechanical fixation of NT10-Sr3

samples was significantly stronger than that of the others, further confirming that the NT10-Sr3 modification enhanced the osseointegration of the implants.

It has been suggested that both topography and dissolution products contribute to the superior bioactivity of NT-Sr coatings on Ti implants. We believe that the release of Sr ions from the NT-Sr coatings, together with the hybrid micro-/nanotopographies, contribute to the superior in vivo bone formation. Our study validated that the topographical features of NT-Sr coatings, besides the ion dissolution products, play a critical role in determining the biofunctionalities of the implant.

Our results indicate that the NT-Sr coatings possess improved bonding strength and superior bonding ability compared with NT coatings and pure Ti. The statistically significant differences in new bone formation found for the NT-Sr coatings with respect to NT-coated and pure Ti samples indicate that this type of implant modification might be a good choice for shortening the healing period for integration of bone implants, eg, dental implants.

Conclusion

Ti implants with a Sr-containing NT coating were developed for dental and orthopedic applications in this study. The coating leads to improved bonding at the bone–implant interface, which is of critical importance to the success of implant placement. The fast in vivo bone formation ability was ascribed to the synergistic effects of the hierarchical hybrid micro-/nanotopography and the dissolution products from the coating. NT10-Sr3 shows the most potential for future use as an implant coating in dental and orthopedic applications.

Acknowledgments

Disclosure
The authors report no conflicts of interest in this work.

References
1. Duffy GP, Berry DJ, Rowland C, Cabanela ME. Primary uncemented total hip arthroplasty in patients <40 years old: 10- to 14-year results using first-generation proximally porous-coated implants. *J Arthroplasty*. 2001;16:140–144.
2. Fini M, Giavaresi G, Torricelli P, et al. Osteoporosis and biomaterial osteointegration. *Biomed Pharmacother*. 2004;58:487–493.
3. Rocca M, Fini M, Giavaresi G, Aldini NN, Giardino R. Osteointegration of hydroxyapatite-coated and uncoated titanium screws in long-term ovariectomized sheep. *Biomaterials*. 2002;23:1017–1023.
4. Zhao L, Liu L, Wu Z, Zhang Y, Chu PK. Effects of micropitted/nanotubular titania topographies on bone mesenchymal stem cell osteogenic differentiation. *Biomaterials*. 2012;33:2629–2641.
5. Tzaphlidou M. The role of collagen in bone structure: an image processing approach. *Micron*. 2005;36:593–601.
6. Crawford GA, Chawla N, Das K, Bose S, Bandyopadhyay A. Microstructure and deformation behavior of biocompatible TiO_2 nanotubes on titanium substrate. *Acta Biomater*. 2007;3:359–367.
7. Oh S, Brammer KS, Li YS, et al. Stem cell fate dictated solely by altered nanotube dimension. *Proc Natl Acad Sci U S A*. 2009;106:2130–2135.
8. Popat KC, Leoni L, Grimes CA, Desai TA. Influence of engineered titania nanotubular surfaces on bone cells. *Biomaterials*. 2007;28:3188–3197.
9. Wang N, Li H, Lu W, et al. Effects of TiO_2 nanotubes with different diameters on gene expression and osseointegration of implants in minipigs. *Biomaterials*. 2011;32:6900–6911.
10. Bjursten LM, Rasmusson L, Oh S, Smith GC, Brammer KS, Jin S. Titanium dioxide nanotubes enhance bone bonding in vivo. *J Biomed Mater Res A*. 2010;92:1218–1224.
11. von Wilmowsky C, Bauer S, Roedl S, Neukam FW, Schmuki P, Schlegel KA. The diameter of anodic TiO_2 nanotubes affects bone formation and correlates with the bone morphogenetic protein-2 expression in vivo. *Clin Oral Implants Res*. 2012;23:359–366.
12. Popat KC, Eltgroth M, Latempa TJ, Grimes CA, Desai TA. Decreased *Staphylococcus epidermis* adhesion and increased osteoblast functionality on antibiotic-loaded titania nanotubes. *Biomaterials*. 2007;28:4880–4888.
13. Zhao L, Wang H, Huo K, et al. Antibacterial nano-structured titania coating incorporated with silver nanoparticles. *Biomaterials*. 2011;32:5706–5716.
14. Balasundaram G, Yao C, Webster TJ. TiO_2 nanotubes functionalized with regions of bone morphogenetic protein-2 increases osteoblast adhesion. *J Biomed Mater Res A*. 2008;84:447–453.
15. Peng L, Mendelsohn AD, LaTempa TJ, Yoriya S, Grimes CA, Desai TA. Long-term small molecule and protein elution from TiO_2 nanotubes. *Nano Lett*. 2009;9:1932–1936.
16. Popat KC, Eltgroth M, La Tempa TJ, Grimes CA, Desai TA. Titania nanotubes: a novel platform for drug-eluting coatings for medical implants? *Small*. 2007;3:1878–1881.
17. Xin Y, Jiang J, Huo K, Hu T, Chu PK. Bioactive $SrTiO_3$ nanotube arrays: strontium delivery platform on Ti-based osteoporotic bone implants. *ACS Nano*. 2009;3:3228–3234.
18. Bonnelye E, Chabadel A, Saltel F, Jurdic P. Dual effect of strontium ranelate: stimulation of osteoblast differentiation and inhibition of osteoclast formation and resorption in vitro. *Bone*. 2008;42:129–138.
19. Coulombe J, Faure H, Robin B, Ruat M. In vitro effects of strontium ranelate on the extracellular calcium-sensing receptor. *Biochem Biophys Res Commun*. 2004;323:1184–1190.
20. Braux J, Velard F, Guillaume C, et al. A new insight into the dissociating effect of strontium on bone resorption and formation. *Acta Biomater*. 2011;7:2593–2603.
21. Capuccini C, Torricelli P, Sima F, et al. Strontium-substituted hydroxyapatite coatings synthesized by pulsed-laser deposition: in vitro osteoblast and osteoclast response. *Acta Biomater*. 2008;4:1885–1893.
22. Yang F, Yang D, Tu J, Zheng Q, Cai L, Wang L. Strontium enhances osteogenic differentiation of mesenchymal stem cells and in vivo bone formation by activating Wnt/catenin signaling. *Stem Cells*. 2011;29:981–991.
23. Peng S, Zhou G, Luk KD, et al. Strontium promotes osteogenic differentiation of mesenchymal stem cells through the Ras/MAPK signaling pathway. *Cell Physiol Biochem*. 2009;23:165–174.
24. Choudhary S, Halbout P, Alander C, Raisz L, Pilbeam C. Strontium ranelate promotes osteoblastic differentiation and mineralization of murine bone marrow stromal cells: involvement of prostaglandins. *J Bone Miner Res*. 2007;22:1002–1010.
25. Fournier C, Perrier A, Thomas M, et al. Reduction by strontium of the bone marrow adiposity in mice and repression of the adipogenic commitment of multipotent C3H10T1/2 cells. *Bone*. 2012;50:499–509.
26. Peng S, Liu XS, Wang T, et al. In vivo anabolic effect of strontium on trabecular bone was associated with increased osteoblastogenesis of bone marrow stromal cells. *J Orthop Res*. 2010;28:1208–1214.
27. Hurtel-Lemaire AS, Mentaverri R, Caudrillier A, et al. The calcium-sensing receptor is involved in strontium ranelate-induced osteoclast apoptosis. New insights into the associated signaling pathways. *J Biol Chem*. 2009;284:575–584.
28. Li Y, Li Q, Zhu S, et al. The effect of strontium-substituted hydroxyapatite coating on implant fixation in ovariectomized rats. *Biomaterials*. 2010;31:9006–9014.
29. Zreiqat H, Ramaswamy Y, Wu C, et al. The incorporation of strontium and zinc into a calcium-silicon ceramic for bone tissue engineering. *Biomaterials*. 2010;31:3175–3184.
30. Gentleman E, Fredholm YC, Jell G, et al. The effects of strontium-substituted bioactive glasses on osteoblasts and osteoclasts in vitro. *Biomaterials*. 2010;31:3949–3956.
31. Park JW, Kim HK, Kim YJ, Jang JH, Song H, Hanawa T. Osteoblast response and osseointegration of a Ti-6Al-4V alloy implant incorporating strontium. *Acta Biomater*. 2010;6:2843–2851.
32. Zhao L, Wang H, Huo K, et al. The osteogenic activity of strontium loaded titania nanotube arrays on titanium substrates. *Biomaterials*. 2013;34:19–29.